Connective Tissue Research

ISSN: 0300-8207 (Print) 1607-8438 (Online) Journal homepage: https://www.tandfonline.com/loi/icts20

Critical-sized cartilage defects in the equine carpus

Eve Salonius, Lassi Rieppo, Mikko J. Nissi, Hertta J. Pulkkinen, Harold Brommer, Anne Brünott, Tuomo S. Silvast, P. René Van Weeren, Virpi Muhonen, Pieter A. J. Brama & Ilkka Kiviranta

To cite this article: Eve Salonius, Lassi Rieppo, Mikko J. Nissi, Hertta J. Pulkkinen, Harold Brommer, Anne Brünott, Tuomo S. Silvast, P. René Van Weeren, Virpi Muhonen, Pieter A. J. Brama & Ilkka Kiviranta (2019) Critical-sized cartilage defects in the equine carpus, Connective Tissue Research, 60:2, 95-106, DOI: 10.1080/03008207.2018.1455670

To link to this article: https://doi.org/10.1080/03008207.2018.1455670

Accepted author version posted online: 21 Mar 2018.
Published online: 12 Apr 2018.

CONNECTIVE TISSUE RESEARCH
2019, VOL. 60, NO. 2, 95–106
https://doi.org/10.1080/03008207.2018.1455670

Taylor & Francis
Taylor & Francis Group

Critical-sized cartilage defects in the equine carpus

Eve Salonius [a], Lassi Rieppo [b,c], Mikko J. Nissi [d], Hertta J. Pulkkinen [e], Harold Brommer [f], Anne Brünott [f], Tuomo S. Silvast [g], P. René Van Weeren [f], Virpi Muhonen [a], Pieter A. J. Brama [h], and Ilkka Kiviranta [a,i]

[a]Department of Orthopaedics and Traumatology, University of Helsinki, Helsinki, Finland; [b]Research Unit of Medical Imaging, Physics and Technology, University of Oulu, Oulu, Finland; [c]Medical Research Center, University of Oulu and Oulu University Hospital, Oulu, Finland; [d]Department of Applied Physics, University of Eastern Finland, Kuopio, Finland; [e]Institute of Biomedicine, University of Eastern Finland, Kuopio, Finland; [f]Department of Equine Sciences, Utrecht University, Utrecht, The Netherlands; [g]SIB Labs, University of Eastern Finland, Kuopio, Finland; [h]Section of Veterinary Clinical Sciences, School of Veterinary Medicine, University College Dublin, Dublin, Ireland; [i]Department of Orthopaedics and Traumatology, Helsinki University Hospital, Helsinki, Finland

ABSTRACT

Aim: The horse joint, due to its similarity with the human joint, is the ultimate model for translational articular cartilage repair studies. This study was designed to determine the critical size of cartilage defects in the equine carpus and serve as a benchmark for the evaluation of new cartilage treatment options. ***Material and Methods***: Circular full-thickness cartilage defects with a diameter of 2, 4, and 8 mm were created in the left middle carpal joint and similar osteochondral (3.5 mm in depth) defects in the right middle carpal joint of 5 horses. Spontaneously formed repair tissue was examined macroscopically, with MR and μCT imaging, polarized light microscopy, standard histology, and immunohistochemistry at 12 months. ***Results***: Filling of 2 mm chondral defects was good (77.8 ± 8.5%), but proteoglycan depletion was evident in Safranin-O staining and gadolinium-enhanced MRI (T_{1Gd}). Larger chondral defects showed poor filling (50.6 ± 2.7% in 4 mm and 31.9 ± 7.3% in 8 mm defects). Lesion filling in 2, 4, and 8 mm osteochondral defects was 82.3 ± 3.0%, 68.0 ± 4.6% and 70.8 ± 15.4%, respectively. Type II collagen staining was seen in 9/15 osteochondral defects but only in 1/15 chondral defects. Subchondral bone pathologies were evident in 14/15 osteochondral samples but only in 5/15 chondral samples. Although osteochondral lesions showed better neotissue quality than chondral lesions, the overall repair was deemed unsatisfactory because of the subchondral bone pathologies. ***Conclusion***: We recommend classifying 4 mm as critical osteochondral lesion size and 2 mm as critical chondral lesion size for cartilage repair research in the equine carpal joint model.

ARTICLE HISTORY
Received 10 October 2017
Revised 3 January 2018
Accepted 3 March 2018
Published online 16 April 2018

KEYWORDS
Animal model; cartilage repair; critical-sized defect; preclinical research; spontaneous repair

Introduction

Animal models are used for the evaluation of the efficacy of new surgical techniques. When investigating articular cartilage repair *in vivo*, joint size and cartilage thickness are considered key factors in defining the most appropriate species (1,2). The joint size, cartilage thickness, and gait mechanics of the horse are closest to those of humans (3,4). Moreover, naturally occurring equine cartilage lesions have similar etiology as human lesions (1,3,4). These similarities allow for a realistic evaluation of novel methods for cartilage repair. In the equine model, stifle, tarsotibial, and carpal joints have been used in translational cartilage repair research. To enable effective use of the equine model in translational cartilage research, the intrinsic repair capacity of equine cartilage in the specific joint must be known.

A critical-sized lesion is a lesion of a size beyond which the defect does not heal spontaneously. Knowledge about critical lesion sizes in animal experiments is necessary for cost reduction and minimizing the suffering of animals while still providing reliable data on the effect of the studied technique. Critical lesion size used in previous equine studies has been defined as lesion size beyond which any void made is not filled (5). However, tissue quality should also be taken into consideration when defining cartilage repair. Aiming at tissue regeneration, that is, restoration of normal tissue architecture and function, instead of merely filling the defects is paramount for achieving durable results (6). Therefore, this kind of defect filling cannot be considered to be successful healing.

There are no recent studies on spontaneous cartilage repair in the equine carpus, and previous studies have generally used basic methods, such as macroscopic inspection, standard histology, and basic biochemistry for the assessment of repair tissue quantity and quality

CONTACT Eve Salonius eve.salonius@helsinki.fi University of Helsinki, Biomedicum Helsinki, Department of Surgery, Haartmaninkatu 8, 00290 Helsinki, Finland.

(5,7). Apart from this, to our knowledge, there are no data on the long-term evolution of artificially made superficial chondral lesions in horses. Given the increasing recognition of the equine model for the evaluation of cartilage repair techniques (1,3,8), and the equine carpus being the most common site of naturally occurring osteoarthritis after metacarpophalangeal joint (9), our study focused on characterization of the long-term spontaneous repair of variably sized chondral and osteochondral defects in the equine carpus using state-of-the-art analytical techniques. As small cartilage defects have been thought to heal well (3,5,8), we hypothesized that the critical defect size would be larger than 2 mm in diameter. The information obtained in this study can be used as a benchmark when evaluating the effect of different techniques aiming at cartilage regeneration in an equine translational model, as it defines to what extent lesions of different sizes will heal spontaneously over a long period (12 months) in the equine carpus.

Methods

Surgical procedure

Five 24-month-old horses (*Equus caballus*) were included in this study. The study was authorized by the Utrecht University Animal Experiments Committee (0412.0601, Utrecht, The Netherlands) in compliance with the Dutch Act on Animal Experimentation. The animal care was in accordance with Utrecht University guidelines. Surgery was performed under general anesthesia following routine clinical procedures. All the horses were assessed clinically and radiologically prior to inclusion in the study and were found to be skeletally mature and to present no abnormalities.

The horses received meloxicam preoperatively (0.6 mg/kg, *i.v.*, Metacam®, Boehringer Ingelheim). The middle carpal joints were approached through a lateral-dorsal and medio-dorsal 1.5–2 cm length arthrotomy to create defects of 2 mm (3 mm^2), 4 mm (13 mm^2), 6 mm (28 mm^2), and 8 mm (50 mm^2) in diameter on the 2nd, 3rd, and 4th carpal bones as shown in Figure 1. Defects were prepunched with a 2, 4, 6, or 8 mm skin biopsy punch. For chondral defects, cartilage was carefully removed with ring curettes onto the level of calcified cartilage (approximately 1 mm in depth) in the left carpus. For osteochondral lesions created in the right carpus, drilling was performed under continuous lavage with Ringer's solution using a hand drill. A 2, 4, 6, or 8 mm pointed drill bit was initially used, followed by a custom-made flattened drill bit of the same size and a custom-made drill sleeve to provide a uniform defect with a flattened bottom and controlled depth of 3.5 mm. Healthy cartilage adjacent to the lesions served as control for all defects.

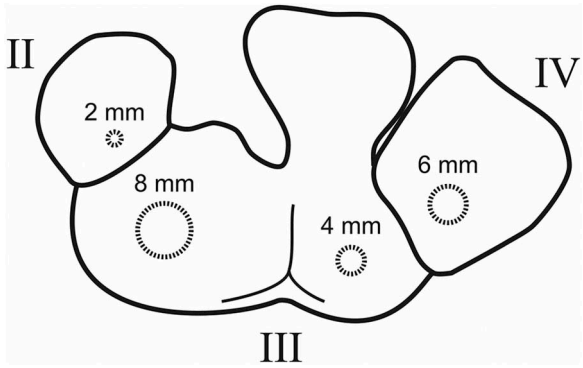

Figure 1. Schematic drawing of the left equine carpal bones II–IV with the four different lesion sizes marked with dashed lines.

Postoperatively, the animals were confined to individual box-stalls (3.5 × 3.5 m) for 2 weeks, after which a gradual 6-week rehabilitation program consisting of incremental controlled walking started. Thereafter, depending on the season and weather conditions, the animals were turned out to pasture or kept in box stalls with daily exercise of 20–30 min in a mechanical horse walker. The exercise regimen was identical for all horses. Synovial fluid and blood samples were collected at weeks 0, 2, 6, 14, 26, 38, and immediately after euthanasia. The total follow-up period was 12 months during which the lesions were allowed to heal spontaneously.

The 6 mm lesions created in *os carpale IV* were used in other studies (10–12). As their processing was different from the other samples, the 6 mm lesions are not included in this study.

Macroscopic evaluation and sample collection

After sacrificing the animals, the carpal joints were opened and macroscopic photographs were taken. Cylindrical osteochondral samples (14 mm in diameter and approximately 1 cm in depth) were taken using a hollow drill that was centered over the original lesion. The samples were frozen and stored at −20°C until further processing.

Micro-computed tomography (μCT)

The samples were thawed in PBS supplemented with inhibitors of metalloproteinases [5 mM ethylenediamine tetraacetic acid (EDTA) disodium salt (VWR International, Fontenay, France) and 5 mM benzamidine hydrochloride (Sigma-Aldrich, St. Louis, MO)],

and analyzed with a SkyScan-1172 scanner (SkyScan, Aartselaar, Belgium). The volume of interest was a cylinder with the diameter of the defect size and height of 6 mm. In control samples, the diameter was 8 mm. The data was analyzed for the structural bone parameters: bone volume fraction (*BV/TV*), trabecular thickness (*Tb.Th*), trabecular spacing (*Tb.Sp*), and trabecular number (*Tb.N*).

Magnetic resonance imaging (MRI)

Thawed samples were MR imaged with a 9.4 T device (Oxford 400 NMR vertical magnet; Oxford Instruments, Witney, England), equipped with a Varian DirectDrive console (VnmrJ 2.3, Varian, Palo Alto, CA, USA) and a 19 mm quadrature volume coil (RAPID Biomedical, Rimpar, Germany). The specimens were placed in a test tube and immersed in saline. T_2 relaxation time was measured in a single slice of 1 mm thickness using a single echo spin echo sequence with TEs of 12, 24, 50, 80, and 110 ms, a TR of 2.5 s and in-plane resolution of 70 × 140 µm. Native T_1 relaxation time was measured in the same slice with the same resolution, using a progressive saturation recovery sequence with TRs of 0.3, 0.6, 1.2, 2.4, and 4.8 s and TE of 11.7 ms. After the first scans, the specimens were immersed in a 1.0 mM Gd-DTPA^{2-} solution for 20 h at room temperature (RT), after which T_{1Gd} was measured using the same saturation recovery sequence with the same resolution, but with TRs of 0.1, 0.2, 0.4, 0.8, and 1.6 s. Two regions of interest (ROIs) were defined in the MR images as exemplified in Figure 2: ROI 1 covered exclusively any repair tissue at the lesion sites of the samples, regardless of its location (repair tissue only). ROI 2 was spatially aligned with the surrounding healthy cartilage and located where the repair tissue assumingly should be if everything was perfectly healed, and further split into superficial and deep halves (upper and lower part of the cartilage). A control ROI was defined in the adjacent healthy tissue and also split into superficial and deep halves.

Polarized light microscopy

After the imaging studies, the samples were processed for histology. The sample cylinders were fixed in 10% formalin for 48 h at RT. The samples were decalcified in 10% EDTA and 4% formaldehyde in 0.1 M phosphate buffer at RT, cut in half, dehydrated in ascending alcohol series, and embedded in paraffin. Tissue sections of 5 µm in thickness were cut from the middle of the lesion.

Unstained tissue sections were measured using polarized light microscopy (Leitz Ortholux II POL, Leitz Wezlar, Wezlar, Germany) (13). The repair tissue was evaluated using a 300-µm-wide ROI, which was divided into 10 layers of equal thicknesses for the analysis. The orientation of collagen fibrils in relation to the cartilage surface (0–90 degrees), and parallelism index (PI), which describes the randomness of fibril orientations within the pixel (0–1, where 0 indicates completely random organization and 1 indicates completely parallel organization) (13), were determined from the most superficial, middle, and the deepest section.

Histological and immunohistological evaluation

Tissue sections were stained with Safranin-O using standard protocols (14). Mosaic images of the histological sections were generated with the Zeiss AxioImager Z1 microscope system equipped with an AxioCam MRc5 camera and Zen blue edition software (Carl Zeiss Microscopy GmbH).

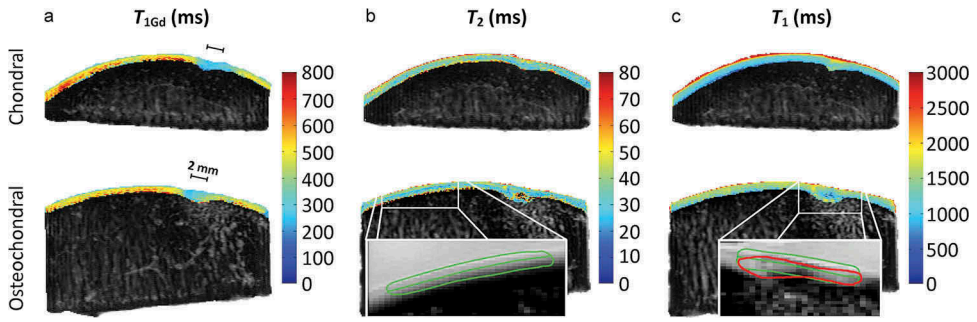

Figure 2. Representative MRI relaxation time maps of the chondral (top row) and osteochondral (bottom row) lesions of 2 mm diameter. Lesion site is immediately below the scale bar (2 mm). Shorter T_{1Gd} relaxation times were observed in both lesions, but more prominently so in the chondral lesion (A). Slight differences as compared to the adjacent tissue were also evident in the T_2 and T_1 relaxation time maps (A, B). The ROI for control tissue is exemplified in the magnification of b. In the magnification of c, the ROI 1 for the repair tissue is marked with red, and the ROI 2 aligned to adjacent healthy cartilage is marked with green.

Lesion filling was calculated from the Safranin-O stained sections using color thresholding in the Fiji program (15). The ROI from which the lesion filling was calculated covered the entire lesion, with the width being the defect diameter and the depth being 1 mm for chondral lesions and 3.5 mm for osteochondral lesions. As the ROI for the osteochondral defects extended into the subchondral bone, the natural trabecular spaces in the sections resulted in empty spaces and thus in a smaller filling degree in the healthy osteochondral control samples than in the chondral samples.

The Safranin-O stained tissue sections in study III were evaluated using the OARSI histopathology score validated for equine cartilage, in which each parameter is evaluated 0–4 where 0 represents healthy cartilage tissue (16). The sections were scored by three independent, blinded observers and an average of the scores was used. The defects that lacked any repair tissue were given the worst score of 4 for each parameter.

A previously published protocol (14) was used to evaluate the staining for type I and type II collagen. Briefly, the sections were digested with hyaluronidase (2 mg/mL, Sigma-Aldrich) and pronase (2 mg/mL, Calbiochem, Merck KGaA), and immersed in hydrogen peroxide (EnVision®+ System-HRP (AEC), Dako North America Inc.) to block endogenous peroxidase activity. Nonspecific staining was blocked with 10% normal goat serum (Dako Denmark A/S, Glostrup, Denmark). The sections were then incubated overnight at 4°C with primary antibodies against collagen type II (ab34712, Abcam) and collagen type I (ab34710), and diluted to 4 µg/mL with PBS supplemented with 1% bovine serum albumin (Sigma-Aldrich). Horseradish peroxidase (HRP)-conjugated goat anti-rabbit secondary antibody (Dako) was then applied. Antibody binding was visualized with AEC substrate chromogen (Dako). The staining of each sample was evaluated under light microscopy.

Statistical analysis

Confidence intervals and standard errors were calculated with the IBM SPSS Statistics 22 software. Osteochondral and chondral lesions of the same diameter were compared to each other. The significances of differences in the µCT, MRI, and polarized light microscopy parameters were evaluated with a pairwise t test, and Sidak adjustment was made for multiple testing. Significances of difference in lesion filling were calculated with permutation type ANOVA testing and Sidak adjustment. Comparisons of lesions and control tissue were made with permutation type ANOVA testing with Dunnet method. A p value under 0.05 was used as the threshold to indicate a statistically significant difference.

Results

Postoperative animal wellbeing

The surgeries were uneventful and all animals recovered well. All the horses demonstrated a pattern of decreasing joint effusion and lameness after surgery that can be expected during the normal healing of an arthrotomy in clinical cases. Joint effusion and lameness were minimal at postoperative day 10 during suture removal and all the horses were fully recovered by 3–4 weeks postsurgery. No clinical abnormalities were noticed in any of the horses during the remainder of the experiment.

Gross appearance of the repair tissue

Most of the 2 mm lesions showed good macroscopic filling (5 of 5 osteochondral and 3 of 5 chondral defects) (Figure 3). The 4 mm lesions were clearly distinguishable from the surrounding healthy cartilage and were incompletely filled. One chondral 4 mm lesion (animal D) showed rather good filling. Each of the 8 mm lesions was incompletely filled. No degenerative changes were detected.

Micro-computed tomography

Visually, the bone structure was normal under the chondral lesions of 2 and 4 mm in diameter (Figure 4). Bone compactness was visually observed to be decreased in 4 of the 5 chondral lesions with a diameter of 8 mm, and one of these samples showed a small subchondral bone erosion. There were subchondral bone changes in all but one of the osteochondral defects (the exception being horse E, 2 mm lesion). Only two osteochondral samples with a diameter of 2 mm presented without cyst-like bone changes. All osteochondral lesions of 4 and 8 mm in diameter had unhealed bone or a cyst-like bone lesion. There were no clear trends in the numeral µCT data and the individual variation between the samples was large. No statistically significant differences were found between the chondral and osteochondral defects but the trabeculae were thinner in osteochondral defects of all sizes than in healthy control tissue ($p = 0.003$).

Magnetic resonance imaging

The relaxation times in ROI 1 (repair tissue only) showed no clear trends with respect to the increasing lesion diameter (Figure 5A). However, T_{1Gd} relaxation times were shorter ($p = 0.014$ and $p < 0.001$ for osteochondral and chondral lesions, respectively) and T_1

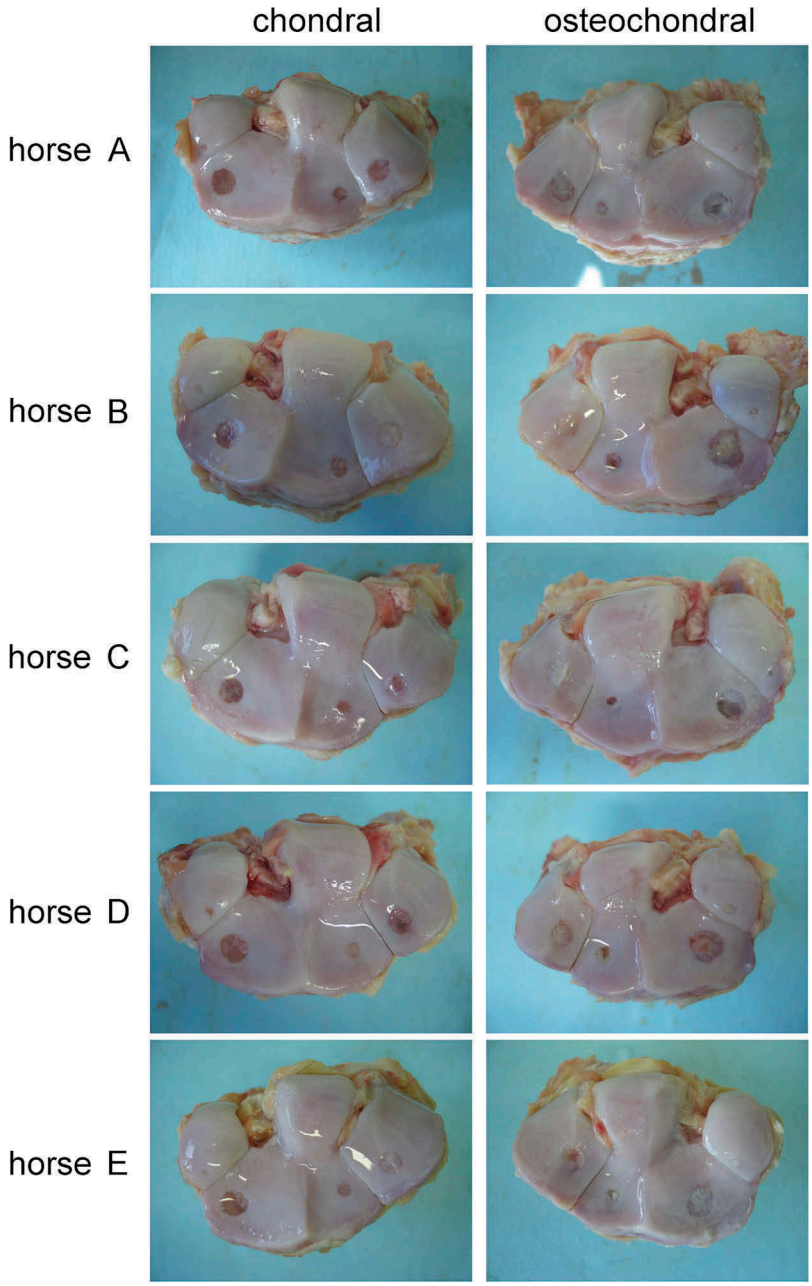

Figure 3. Photographs of the joints taken directly after sacrificing the animals. Chondral lesions are in the left column and osteochondral in the right column. Each horse is represented in its own row. Macroscopically, 5 of 5 osteochondral and 3 of 5 chondral lesions with the diameter of 2 mm were filled with repair tissue. Of the 4 mm lesions, only one chondral lesion (horse D) was well filled, the other lesions were easily distinguishable and not filled to the level of the surrounding cartilage. Each 8 mm defect was clearly visible but one osteochondral defect (horse E) showed good filling in the middle of the lesion.

relaxation times slightly longer ($p = 0.156$ and $p = 0.037$ for osteochondral and chondral lesions, respectively) in the repair tissues than in the control samples (Figure 5).

In all ROIs, the osteochondral lesions had longer T_{1Gd} relaxation times than the chondral lesions, indicative of a higher proteoglycan content. However, no statistically significant differences were observed. In ROI 1, the T_2 relaxation time was shorter in the 8 mm wide osteochondral defects than in the chondral defects (33.8 ± 0.8 ms for osteochondral and 41.0 ± 1.3 ms for chondral lesions, $p = 0.020$). ROI 2 (lesion area aligned to adjacent healthy cartilage) showed increasing T_2s with larger lesion diameters and toward the cartilage surface. Osteochondral lesions with a diameter of 8 mm deviated from this trend and showed lower T_2 values (48.9 ± 8.4 ms) than the 4 mm lesions (59.2 ± 10.3 ms). The 8 mm lesions also demonstrated a significant difference between the

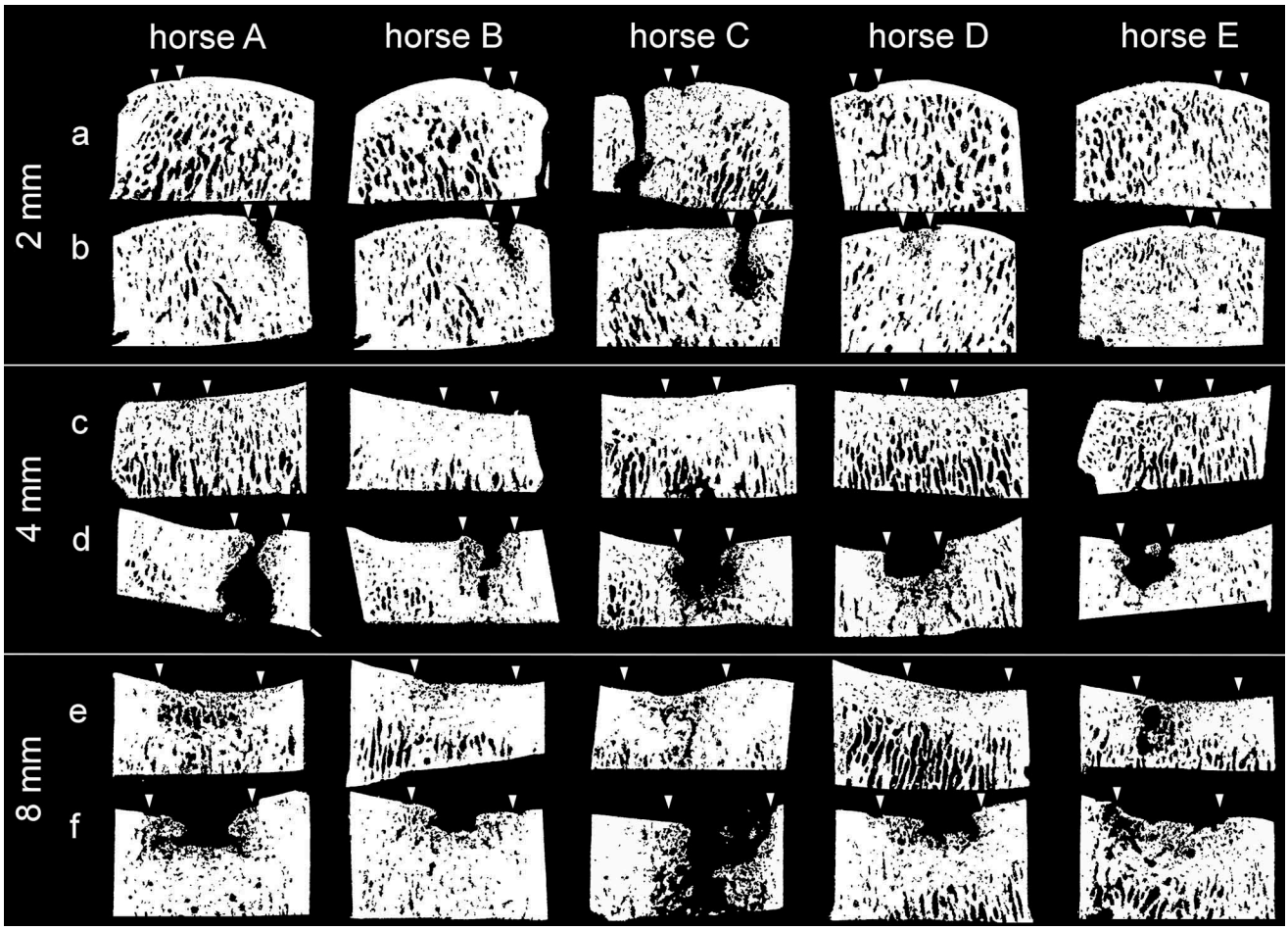

Figure 4. Micro-computational tomographic image of the middle part of each specimen. The osteochondral lesions (b, d, f) presented with subchondral bone resorption, whereas the bone structure in the chondral lesions (a, c, e) was either undisturbed or slightly decreased in density. Arrowheads show the site of the original defect.

osteochondral and chondral samples in the deep part of ROI 2 (103.9 ± 12.2 ms for chondral and 48.9 ± 8.4 ms for osteochondral defects, respectively, $p = 0.020$).

The T_1 relaxation time of the chondral samples in ROI 2 showed a trend of increasing with lesion diameter and from the deep part of the tissue toward the cartilage surface (Figure 5B and C). The T_1 relaxation times of all chondral lesions were higher than those of the control tissue ($p < 0.001$). The largest variation in T_1 relaxation time was noted for osteochondral lesions with a diameter of 8 mm. T_1 relaxation time did not show significant differences between the groups in either of the ROIs.

Changes in the relaxation times were visually observed, especially in the T_{1Gd} relaxation time between the lesion sites and adjacent tissue, exemplified here in the cases of the 2 mm lesions (Figure 2). While the relaxation times of the subchondral bone are not shown, also differences in the MRI signal of the subchondral bone immediately below the lesion site were observed between the lesion types: a uniform appearance of the signal is seen below the chondral lesions, while an area of increased signal was present in the vicinity of the osteochondral lesions, indicating an increased water content in the area (Figure 2).

Polarized light microscopy

Polarized light microscopy showed high PIs in all samples (Figure 6). Chondral lesions with a diameter of 2 mm showed a higher parallelism of collagen fibrils than osteochondral lesions in the deep part of the repair tissue (0.891 ± 0.02 for chondral and 0.787 ± 0.03 for osteochondral lesions, $p = 0.042$). Otherwise, no statistically significant differences in the PI between the lesion diameters or the lesion depths were detected.

Collagen orientation showed large variations between the groups and between individual samples. Collagen orientation changed toward the typical tangential orientation in the superficial part of the 2 mm lesions (Figure 7A) and deviated from what was expected in the larger lesions. The osteochondral samples showed a

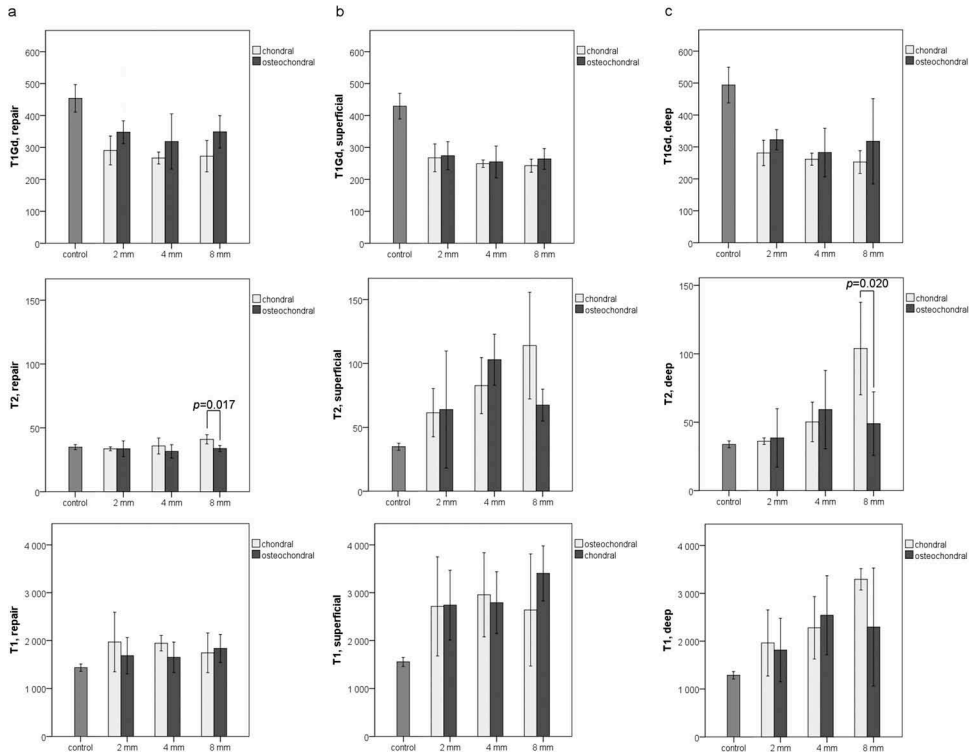

Figure 5. Mean relaxation time values (ms) of the magnetic resonance imaging in the different cartilage ROIs. Results for the repair tissue only (ROI 1) in each group are shown in (A), and the area aligned to the adjacent healthy cartilage (ROI 2) was divided into a superficial half (B) and deep half (C). Chondral lesions are colored white and osteochondral ones dark gray. The whiskers represent 95% confidence interval. Statistically significant *p* values are marked in the images.

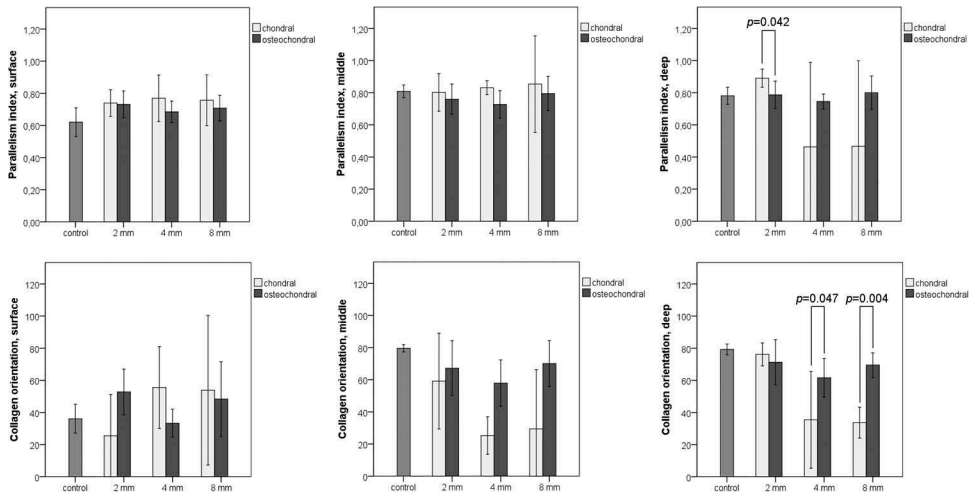

Figure 6. Bar diagrams showing the mean parallelism index (PI, top row) of the collagen fibrils and the mean orientation (bottom row) of the fibrils. Chondral lesions are colored white and osteochondral lesions dark gray. The whiskers represent 95% confidence interval. Statistically significant *p* values are marked in the images.

higher level of fibril organization than the chondral samples in the deep part of the tissue, the collagen orientation being 61.6 ± 4.3° for 4 mm and 69.5 ± 2.7° for 8 mm osteochondral defects, and 35.4 ± 7.0° for 4 mm and 33.6 ± 2.2° for 8 mm chondral defects (p = 0.047 and p = 0.004 for 4 and 8 mm lesions, respectively).

Histological repair quality

Lesion filling was analyzed from the Safranin-O stained sections. Filling of the osteochondral control samples was 81.7 ± 0.2% and filling of chondral controls was 99.4 ± 4.7%. Lesion filling was most complete

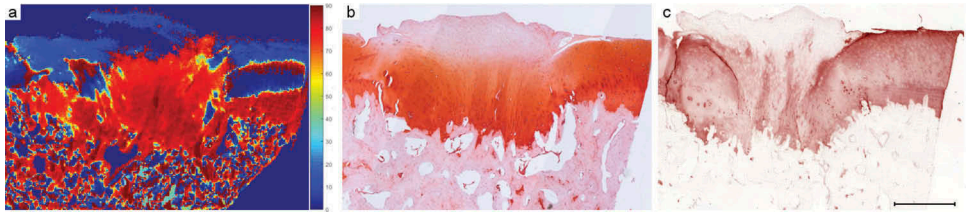

Figure 7. Representative osteochondral defect with a diameter of 2 mm. (A) Polarized light microscopy showed the change in collagen orientation toward the typical tangential orientation in the superficial layer. (B) Safranin-O staining showed good filling and abundant proteoglycans in the deep part of the repaired cartilage tissue. (C) Immunohistochemical staining for type II collagen. Scale bar: 500 µm.

(82.3 ± 3.0%) in the osteochondral lesions in which the repair tissue reached the level of the surrounding cartilage surface in all of the 2 mm lesions (Figures 7 and 8). On the other hand, 4 of 5 of the 4 mm lesions and 1 of 5 of the 8 mm lesions presented with repair tissue nonaligned with the surrounding cartilage with filling of 68.0 ± 4.6% for 4 mm osteochondral defects and 70.8 ± 15.4% for 8 mm defects, respectively. All of the 2 mm chondral lesions showed good lesion filling (77.8 ± 8.5%) whereas filling of the 4 mm chondral defects was 50.6 ± 2.7% and filling of the 8 mm defects was 31.9 ± 7.3%. Nine of 10 of the 4 and 8 mm lesions showed only small islands of unstained repair tissue or even a complete absence of repair cartilage in the histological sections. Islands of repair tissue occurred at sites where the subchondral bone plate was disrupted (Figure 8). None of the defects showed lateral expansion. The filling of osteochondral samples did not differ from healthy control cartilage ($p = 0.085$) whereas the filling of the chondral samples differed from the controls ($p < 0.001$).

More than half of the osteochondral lesions in each diameter category showed repair tissue with good

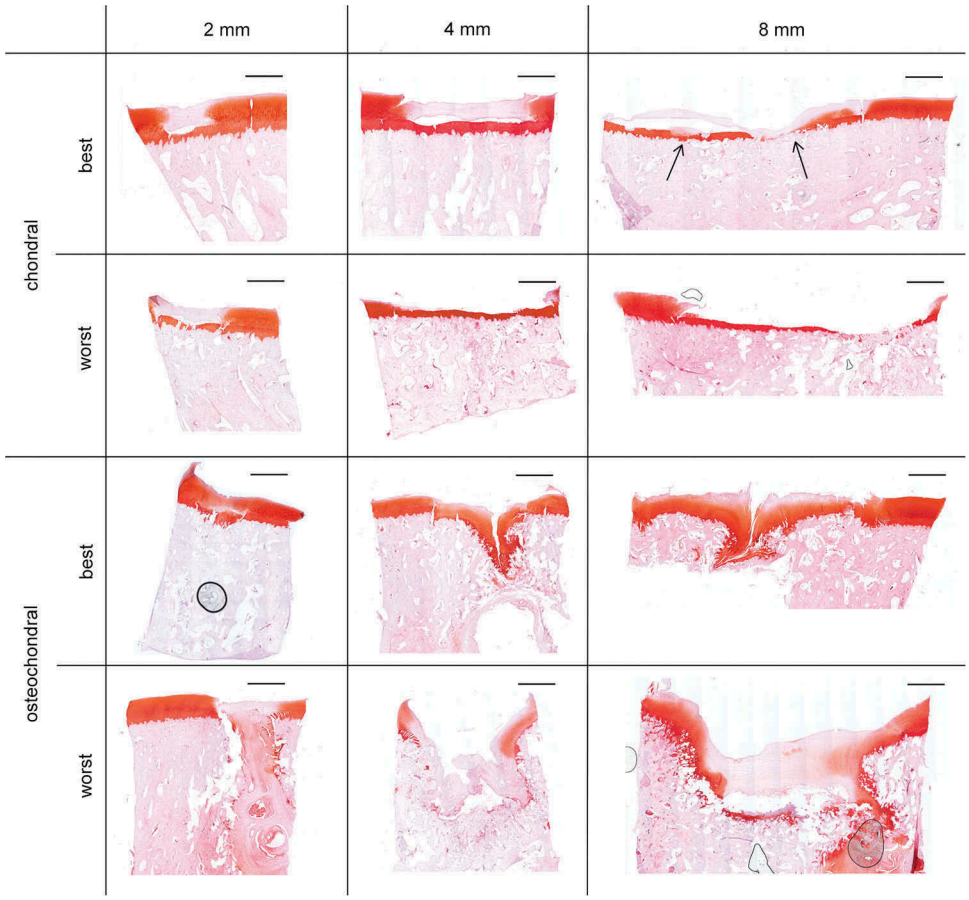

Figure 8. The best and worst Safranin-O stained histological section in each study group. Repair tissue seemed to originate partly from the subchondral bone at the sites where the calcified cartilage was disrupted (arrows). Scale bars: 1 mm.

Safranin-O stain uptake whereas only one of the chondral lesions showed Safranin-O positive tissue at the repair site (Table 2). As the repair tissue was absent from two 4 mm chondral lesion and four 8 mm chondral lesion samples, those samples were perceived negative for Safranin-O uptake. Typically, the osteochondral samples showed hyaline-like cartilage in the deep or middle part of the repair tissue and fibrous tissue on the surface. The best and the worst repairs in each group are shown in Figure 8.

Typically, osteochondral defects showed lower values of OARSI score than chondral defects (Table 1). This is indicative of better tissue quality in the osteochondral samples. Loss of Safranin-O uptake was common in all of the defect sizes. No degenerative changes were detected in the control cartilage adjacent to the lesions.

Immunohistochemistry

Almost all of the 2 mm osteochondral samples (4 of 5) showed positive type II collagen staining and only one of these samples showed positive type I collagen staining (Figure 7, Table 2). In the 2 mm chondral samples, positive staining for type II and type I collagen was shown in 1 of 5 and 4 of 5 samples, respectively. Fibrocartilage formation was evident in the larger chondral and osteochondral lesions where a mixture of type I and type II collagen positive tissue was present. Since the repair tissue was detached from two of the 4 mm chondral lesions and four of the 8 mm chondral lesions, these were perceived negative for both type I and II collagen.

Discussion

The purpose of this study was to determine the intrinsic repair capacity of equine carpal articular cartilage to set a benchmark for studies evaluating articular cartilage repair strategies using the equine carpus as a model. Knowledge on spontaneous repair capacity and critical lesion size improves cost-effectiveness and minimizes animal suffering in animal experiments. The quality and quantity of the repair tissue in both chondral and osteochondral defects were evaluated in this study. Complete tissue regeneration was not achieved as the repair tissue structure differed from healthy cartilage in all the defects. Only the osteochondral lesions with 2 mm diameter showed good Safranin-O staining indicating a good quality of the repair tissue, while equally sized chondral defects failed to spontaneously repair to hyaline cartilage. Chondral defects and osteochondral defects with the diameter of 4 and 8 mm showed depletion of proteoglycans and structural disorganization.

The healing of equine carpal cartilage defects was first described by Riddle (17) who created superficial and full-thickness defects in the carpus of four horses (150 mm^2) and six ponies (100 mm^2). He concluded that the superficial defects did not heal past the 8-month time point and that in order for the defects to heal, they should reach the subchondral bone. The importance of the connection to the bone marrow spaces has since been confirmed by others (18,19). Mean filling of both untreated and microfracture-treated chondral defects of 100 mm^2 in equine carpus in the study by Frisbie was, however, only 65% or less (18).

Table 1. Results of the OARSI microscopic scoring system (16) for each study group. Each parameter was evaluated 0–4 where 0 represents healthy cartilage tissue. The values are presented as mean ± standard error (SE).

	Chondrocyte necrosis	Cluster formation	Fibrillation/fissuring	Focal cell loss	Loss of Safranin-O
Chondral					
Control	0.84 ± 0.13	0.80 ± 0.12	0.13 ± 0.05	0.00 ± 0.00	0.07 ± 0.04
2 mm	0.55 ± 0.16	0.36 ± 0.14	1.36 ± 0.15	1.76 ± 0.19	3.76 ± 0.11
4 mm	3.72 ± 0.14	3.11 ± 0.27	3.14 ± 0.26	3.47 ± 0.17	4.00 ± 0.00
8 mm	2.91 ± 0.24	2.53 ± 0.28	3.16 ± 0.20	3.02 ± 0.21	3.91 ± 0.04
Osteochondral					
Control	0.24 ± 0.08	0.53 ± 0.10	1.16 ± 0.12	0.07 ± 0.04	0.22 ± 0.06
2 mm	1.51 ± 0.20	0.71 ± 0.12	1.29 ± 0.15	1.29 ± 0.16	2.02 ± 0.20
4 mm	2.22 ± 0.21	1.37 ± 0.19	2.15 ± 0.14	2.22 ± 0.16	3.35 ± 0.11
8 mm	0.59 ± 0.11	0.47 ± 0.11	1.69 ± 0.16	1.24 ± 0.13	3.25 ± 0.10

Table 2. Number of specimens with positive staining for Safranin-O or immunohistochemical staining for type I and type II collagen in each lesion type. As the repair tissue was detached from two of the 4 mm chondral lesions and four of the 8 mm chondral lesions, those samples were perceived negative for Safranin-O and type I and II collagen.

	2 mm		4 mm		8 mm	
	Chondral	Osteochondral	Chondral	Osteochondral	Chondral	Osteochondral
Safranin-O	1/5	4/5	0/5	4/5	0/5	3/5
Type I collagen	4/5	1/5	2/5	2/5	1/5	2/5
Type II collagen	1/5	4/5	0/5	2/5	0/5	3/5

In a study evaluating spontaneous healing of full-thickness cartilage defects in the equine carpus by Hurtig et al. (5), lesions with a surface area of 5 mm^2 were filled with fibrocartilaginous repair tissue but lesions of 15 mm^2 deteriorated to dense fibrous tissue. This is corroborated by our study, where nearly all full-thickness chondral defects of 3 mm^2 (2 mm in diameter) showed fibrocartilaginous repair, and larger defects presented with incomplete fibrocartilage covering or no repair tissue at all.

Spontaneous defect healing reported in previous equine studies is mainly described as filling of the lesions or formation of fibrous tissue and fibrocartilage (5,20). Fibrocartilage, however, has lower mechanical strength than hyaline cartilage and as such, it is more prone to wearing out (21). Durable, long-lasting results can only be achieved by restoration of fully functional hyaline cartilage (6). The focus of interventions aiming at cartilage repair has shifted from simply filling the lesions to restoring mature hyaline cartilage. In order to reliably determine the critical lesion size, it is paramount to evaluate both the quantity and quality of repair tissue. In the present study, only the osteochondral defects showed hyaline-like repair tissue with higher proteoglycan content and better filling after a 12-month follow-up (Figures 4 and 8). Even though small full-thickness chondral defects have been thought to heal spontaneously (3,5,8), the results of this study suggest otherwise. Although the filling in the 2 mm defects was good macroscopically, depletion of proteoglycans was evident both in Safranin-O staining and gadolinium-enhanced MR imaging (T_{1Gd}). Structural disorganization and fibrocartilage formation were seen in polarized light microscopy and as a mixture of type I and II collagen staining in immunohistochemistry, and low T_2 and T_{1Gd} values in MRI (22,23). The deep part of the repair tissue in the osteochondral defects showed a structure closely resembling that of the healthy control tissue in polarized light microscopy, whereas the chondral defects showed poorly organized tissue in each layer, implying a mechanically weaker tissue structure. These findings substantiate the previous studies that show that the repair tissue originates from the bone marrow (24) and explain the poor outcome of the chondral defects.

Although the osteochondral defects showed better repair than chondral defects, the bone voids of the deep osteochondral defects did not heal or even became larger, extending up to 9 mm into the bone, during the 12-month follow-up. Even the smallest 2 mm osteochondral lesions showed bone pathologies at the time of the post mortem analysis (4 of 5 specimens). Frequent cyst formation after a disruption of subchondral bone has been reported in previous equine studies (18,25). The present study makes no exception: chondral lesions presented with no cysts whereas bone defects were detected in osteochondral lesions of all sizes (2, 4, and 8 mm).

The long-term follow-up time of 12 months in this study gives a better understanding of the spontaneous repair capacity of equine carpal joint cartilage than the shorter time periods of previous studies on spontaneous repair (8,26). Additionally, this study has several methodological benefits, as current state-of-art methods were used in assessing the repair tissue quality. The tissue was evaluated prior to any processing macroscopically and with μCT and MRI. The outcome of polarized light microscopy reflects the mechanical strength of the repair tissue (27,28). Finally, the overall quality of the repair tissue was assessed with histological and immunohistochemical techniques. The findings of different methods support each other.

There were some limitations in this study. Since defects were created in different sites of the joint, they were subjected to different weight-bearing conditions (7,8). All defects with the same diameter were, however, located on the same site and thus the comparison between chondral and osteochondral defects is justified. The third carpal bone, where the 4 and 8 mm defects were located, bears most weight and is the site in the equine carpus that is most frequently affected by cartilage pathologies (29). Nonetheless, not even the 2 mm lesions located on the less weight-bearing second carpal bone healed well.

Altogether four defects were created in the middle carpal joint of the horses. The combined area of these defects was 94 mm^2, which might possibly have affected the repair of the individual lesions, although degenerative changes were absent around the lesions or on the articulating surfaces. Further, it is not uncommon to create more defects per joint when using the equine model (30,31). In our study in the carpus, none of the lesions with a diameter of 4 mm (13 mm^2) or 8 mm (50 mm^2) healed with mature hyaline cartilage. Even the smallest 2 mm in diameter (3 mm^2) lesions, which were initially thought to serve as the control lesions with good spontaneous healing showed repair tissue of questionable quality at 12 months.

Conclusion

The horse is a good animal model for cartilage research and, like humans, it has a very limited spontaneous healing capacity. Based on this study, we recommend using 4 mm diameter as the critical size for osteochondral lesions and 2 mm diameter lesion as the critical size for chondral lesions in articular cartilage repair research using the equine carpal joint model.

Acknowledgments

The authors wish to thank Outi Kiekara (Department of Anatomy, University of Eastern Finland, Kuopio, Finland) for μCT and MR imaging. We thank Nora Rauhala (Department of Applied Physics, University of Eastern Finland, Kuopio, Finland) for conducting the ROI analyses on the MRI data and Eija Rahunen (Department of Anatomy, University of Eastern Finland, Kuopio, Finland) for technical assistance with histological sample preparation. The Biomedicum Imaging Unit (Faculty of Medicine, University of Helsinki) is acknowledged for microscopy services and Hannu Kautiainen (Medcare Oy, Äänekoski, Finland) for the statistical analyses.

Disclosure statement

The authors report no conflict of interest. The authors alone are responsible for the content and writing of the article.

Funding

This study was funded by the Academy of Finland (Grant #285909) and the Finnish Funding Agency for Innovation Tekes (Grant 3344/31/03). The funding sources had no role in the study design, collection, analysis and interpretation of data; in the writing of the manuscript; and in the decision to submit the manuscript for publication.

ORCID

Eve Salonius http://orcid.org/0000-0003-1988-2800

References

1. Ahern BJ, Parvizi J, Boston R, Schaer TP. Preclinical animal models in single site cartilage defect testing: a systematic review. Osteoarthritis Cartilage 2009 Jun;17(6):705–713.
2. Moran CJ, Ramesh A, Brama PA, O'Byrne JM, O'Brien FJ, Levingstone TJ. The benefits and limitations of animal models for translational research in cartilage repair. J Exp Orthop 2016 Dec;3(1):1.
3. Chu CR, Szczodry M, Bruno S. Animal models for cartilage regeneration and repair. Tissue Eng Part B Rev 2010 Feb;16(1):105–115.
4. Malda J, Benders KE, Klein TJ, De Grauw JC, Kik MJ, Hutmacher DW, Saris DB, van Weeren PR, Dhert WJ. Comparative study of depth-dependent characteristics of equine and human osteochondral tissue from the medial and lateral femoral condyles. Osteoarthritis Cartilage 2012 Oct;20(10):1147–1151.
5. Hurtig MB, Fretz PB, Doige CE, Schnurr DL. Effects of lesion size and location on equine articular cartilage repair. Can J Vet Res 1988 Jan;52(1):137–146.
6. Bernhard JC, Vunjak-Novakovic G. Should we use cells, biomaterials, or tissue engineering for cartilage regeneration?. Stem Cell Res Ther 2016 Apr 18;7(1):56-016-0314-3.
7. Convery FR, Akeson WH, Keown GH. The repair of large osteochondral defects. An experimental study in horses. Clin Orthop Relat Res 1972 Jan-Feb;82:253–262.
8. McIlwraith CW, Fortier LA, Frisbie DD, Nixon AJ. Equine models of articular cartilage repair. Cartilage 2011 Oct;2(4):317–326.
9. McIlwraith CW, Frisbie DD, Kawcak CE. The horse as a model of naturally occurring osteoarthritis. Bone Joint Res 2012 Nov 1;1(11):297–309.
10. Viren T, Huang YP, Saarakkala S, Pulkkinen H, Tiitu V, Linjama A, Kiviranta I, Lammi MJ, Brünott A, Brommer H, Van Weeren R, Brama PA, Zheng YP, Jurvelin JS, Töyräs J. Comparison of ultrasound and optical coherence tomography techniques for evaluation of integrity of spontaneously repaired horse cartilage. J Med Eng Technol 2012 Apr;36(3):185–192.
11. Kulmala KA, Pulkkinen HJ, Rieppo L, Tiitu V, Kiviranta I, Brunott A, Brommer H, van Weeren R, Brama PA, Mikkola MT, Korhonen RK, Jurvelin JS, Toyras J. Contrast-enhanced micro-computed tomography in evaluation of spontaneous repair of equine cartilage. Cartilage 2012 Jul;3(3):235–244.
12. Rautiainen J, Lehto LJ, Tiitu V, Kiekara O, Pulkkinen H, Brunott A, Weeren RV, Brommer H, Brama PAJ, Ellermann J, Kiviranta I, Nieminen MT, Nissi MJ. Osteochondral repair: evaluation with sweep imaging with Fourier transform in an equine model. Radiology 2013 Oct;269(1):113–121.
13. Rieppo J, Hallikainen J, Jurvelin JS, Kiviranta I, Helminen HJ, Hyttinen MM. Practical considerations in the use of polarized light microscopy in the analysis of the collagen network in articular cartilage. Microsc Res Tech 2008 Apr;71(4):279–287.
14. Muhonen V, Salonius E, Haaparanta AM, Jarvinen E, Paatela T, Meller A, Hannula M, Björkman M, Pyhältö T, Ellä V, Vasara A, Töyräs J, Kellomäki M, Kiviranta I. Articular cartilage repair with recombinant human type II collagen/polylactide scaffold in a preliminary porcine study. J Orthop Res 2016 May;34(5):745–753.
15. Schindelin J, Arganda-Carreras I, Frise E, Kaynig V, Longair M, Pietzsch T, Preibisch S, Rueden C, Saalfeld S, Schmid B, Tinevez JY, White DJ, Hartenstein V, Eliceiri K, Tomancak P, Cardona A. Fiji: an open-source platform for biological-image analysis. Nat Methods 2012 Jun 28;9(7):676–682.
16. McIlwraith CW, Frisbie DD, Kawcak CE, Fuller CJ, Hurtig M, Cruz A. The OARSI histopathology initiative - recommendations for histological assessments of osteoarthritis in the horse. Osteoarthritis Cartilage 2010 Oct;18(Suppl 3):S93–105.
17. We R Jr. Healing of articular cartilage in the horse. J Am Vet Med Assoc 1970 Dec 1;157(11):1471–1479.
18. Frisbie DD, Trotter GW, Powers BE, Rodkey WG, Steadman JR, Howard RD, Park RD, McIlwraith CW. Arthroscopic subchondral bone plate microfracture technique augments healing of large chondral defects in the radial carpal bone and medial femoral condyle of horses. Vet Surg 1999 Jul-Aug;28(4):242–255.
19. Vachon A, Bramlage LR, Gabel AA, Weisbrode S. Evaluation of the repair process of cartilage defects of the equine third carpal bone with and without

subchondral bone perforation. Am J Vet Res 1986 Dec;47(12):2637–2645.
20. Vachon AM, McIlwraith CW, Trotter GW, Norrdin RW, Powers BE. Morphologic study of repair of induced osteochondral defects of the distal portion of the radial carpal bone in horses by use of glued periosteal autografts [corrected]. Am J Vet Res 1991 Feb;52 (2):317–327.
21. Hunziker EB. The elusive path to cartilage regeneration. Adv Mater 2009 Sep 4;21(32–33):3419–3424.
22. Nieminen MT, Nissi MJ, Mattila L, Kiviranta I. Evaluation of chondral repair using quantitative MRI. J Magn Reson Imaging 2012 Dec;36(6):1287–1299.
23. Nissi MJ, Toyras J, Laasanen MS, Rieppo J, Saarakkala S, Lappalainen R, et al. Proteoglycan and collagen sensitive MRI evaluation of normal and degenerated articular cartilage. J Orthop Res 2004 May;22(3):557–564.
24. Shapiro F, Koide S, Glimcher MJ. Cell origin and differentiation in the repair of full-thickness defects of articular cartilage. J Bone Joint Surg Am 1993 Apr;75 (4):532–553.
25. Kold SE, Hickman J, Melsen F. An experimental study of the healing process of equine chondral and osteochondral defects. Equine Vet J 1986 Jan;18(1):18–24.
26. Frisbie DD, Lu Y, Kawcak CE, DiCarlo EF, Binette F, McIlwraith CW. In vivo evaluation of autologous cartilage fragment-loaded scaffolds implanted into equine articular defects and compared with autologous chondrocyte implantation. Am J Sports Med 2009 Nov;37 (Suppl 1):71S–80S.
27. Vasara AI, Hyttinen MM, Lammi MJ, Lammi PE, Langsjo TK, Lindahl A, Peterson L, Kellomäki M, Konttinen YT, Helminen HJ, Kiviranta I. Subchondral bone reaction associated with chondral defect and attempted cartilage repair in goats. Calcif Tissue Int 2004 Jan;74(1):107–114.
28. Julkunen P, Harjula T, Iivarinen J, Marjanen J, Seppanen K, Narhi T, Arokoski J, Lammi MJ, Brama PA, Jurvelin JS, Helminen HJ. Biomechanical, biochemical and structural correlations in immature and mature rabbit articular cartilage. Osteoarthritis Cartilage 2009 Dec;17(12):1628–1638.
29. Palmer JL, Bertone AL, Litsky AS. Contact area and pressure distribution changes of the equine third carpal bone during loading. Equine Vet J 1994 May;26 (3):197–202.
30. Hurtig M, Pearce S, Warren S, Kalra M, Miniaci A. Arthroscopic mosaic arthroplasty in the equine third carpal bone. Vet Surg 2001 May-Jun;30(3):228–239.
31. Nixon AJ, Rickey E, Butler TJ, Scimeca MS, Moran N, Matthews GL. A chondrocyte infiltrated collagen type I/III membrane (MACI(R) implant) improves cartilage healing in the equine patellofemoral joint model. Osteoarthritis Cartilage 2015 Apr;23(4):648–660.